Large magnetic moment enhancement and extraordinary Hall effect in Co/Pt superlattices

C. L. Canedy,* X. W. Li,[†] and Gang Xiao

Department of Physics, Brown University, Providence, Rhode Island 02912

(Received 27 September 1999)

High quality (111) and (100) oriented Co/Pt superlattices have been prepared using the magnetron sputtering technique. The extraordinary Hall effect and magnetic properties in a series of these Co/Pt superlattices have been studied. We have established the existence of a large enhanced moment at the Co/Pt interfaces. Tensile strain in the magnetic layers is found to dominate the perpendicular magnetic anisotropy for the (111) orientation. From a systematic variation of the Co layer thickness we have determined that the extraordinary Hall resistivity is dominated by interface scattering. Further, large deviations from the commonly used scaling relations linking the extraordinary Hall resistivity and the ordinary resistivity are observed. These are discussed within a model proposed by Zhang.

I. INTRODUCTION

Artificially layered magnetic structures have received much attention both for their potential device applications and for their wealth of interesting physics.[1] Indeed, they have been shown to exhibit a wide range of exciting phenomena,[2] such as perpendicular magnetic anisotropy (PMA), giant magnetoresistance, and oscillatory exchange coupling. Magnetic studies performed on transition-metal magnetic superlattices, e.g., Co/Au,[3] Co/Cu,[4] Fe/Ag,[5] Co/Pt,[6] and Co/Pd,[7] have revealed that at small magnetic layer thickness, i.e., less than a few monolayers (ML's), the easy axis of magnetization rotates out of the plane of the film. This allows for the attractive possibility of magneto-optical recording media at high recording density. The PMA originates from the interfaces in superlattice systems. However, a clear understanding is lacking and in particular its dependence on interface sharpness, crystal texture, and lattice strain is not well understood.

Another exciting subject in these superlattice systems is their magnetotransport properties. Giant magnetoresistance (GMR) has been extensively studied in metallic superlattices.[8] Another magnetotransport property, which has received relatively little attention, is the extraordinary Hall effect (EHE). Typically, EHE is much larger than the ordinary Hall effect and has potential applications in data storage and magnetic sensing.[9] It remains unclear whether the simple scaling laws, correlating the extraordinary Hall coefficient with the longitudinal resistivity in ferromagnets,[10] are applicable to these superlattice systems. The scaling laws were derived from homogeneous systems such as magnetic alloys, whereas superlattices are heterogeneous systems. Indeed, there have been some experimental and theoretical evidences which point to a more complicated dependence in superlattices.[11–16] So far, there is a lack of systematic studies on EHE in superlattice systems. The EHE arises from the spin-orbit interaction and is directly proportional to the macroscopic magnetization.[10] Thus a system such as Co/Pt, which is known to have both a perpendicular magnetic anisotropy and a substantial Kerr rotation[17] due to a large spin-orbit coupling via the Pt atoms, would seem to be a good candidate for understanding the EHE in layered structures.

In this paper, we report on a systematic study of the structure, magnetic properties, and EHE in Co/Pt superlattices. x-ray-diffraction analysis has revealed the high quality layered structure of both (111) and (100) Co/Pt superlattices grown by the sputtering technique. Magnetic measurements have shown a large PMA at a certain layer thickness range. This property is particularly useful for any applications based on EHE. We assign strain anisotropy as the essential ingredient. We have obtained a giant Co magnetic moment at the Co/Pt interface, which is 155% larger than that of the bulk Co moment. We have systematically investigated the EHE in Co/Pt superlattices over a large thickness range. Conventional EHE scaling laws cannot account for the thickness dependence of EHE in our systems. We have found that the prediction of a different model of EHE for superlattices proposed by Zhang is in qualitative agreement with our results. Further, interface scattering is shown to dominate EHE for these Co/Pt superlattices.

II. EXPERIMENT

Magnetic Co/Pt superlattices were prepared using the magnetron-sputtering technique. A particular superlattice is specified by Co_{N_1}/Pt_{N_2}, where N_1 and N_2 are the number of atomic planes of Co and Pt, respectively, in each bilayer. Typically a 10–20-nm seed layer of Pt was deposited on heated ($\sim 600\,°C$) magnesium oxide (100) or sapphire (0001) substrates to promote epitaxial growth. The superlattices were deposited at about 100–200 °C using a computer monitored sputtering system. The sputtering rate is less than 0.5 Å/s. Before deposition, the background pressure was better than 7×10^{-8} Torr. All samples were capped with 40–50-Å Pt to avoid oxidation. The layer structure of each sample was then determined using a θ–2θ Philips APD 3720 x-ray diffractometer. We have also measured rocking curves on some samples using a Siemens D5000 high-resolution x-ray diffractometer. Standard photolithography and physical etching were used to pattern the samples into Hall bars for transport measurements performed in a cryostat equipped with an 8-T superconducting magnet. In addition, our samples were magnetically characterized using a Quantum Design superconducting quantum interference device magnetometer.
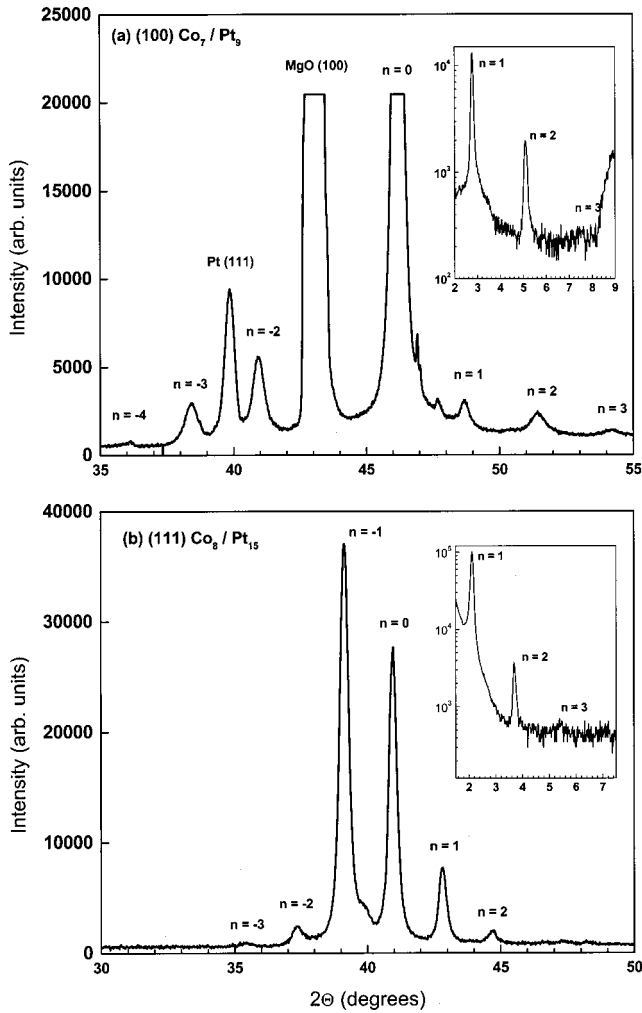
FIG. 1. High angle and low angle x-ray-diffraction patterns for (a) (100) orientated Co_7/Pt_9 superlattice deposited on MgO (001) and (b) (111) orientated Co_8/Pt_{15} superlattice deposited on Al_2O_3 (0001).

III. STRUCTURAL ANALYSIS

Successful growth of Co/Pt superlattices using a high-energy deposition process such as sputtering depends critically on fabrication parameters. Indeed, the quality of the superlattice can be greatly affected by deposition rate, sputtering gas, type of substrate, and deposition temperature.[18] A judicious choice of these processing conditions is necessary to obtain superlattices with optimized magnetic properties and structural characteristics. In Fig. 1 we show representative x-ray-diffraction patterns for (100) and (111) orientated Co/Pt superlattices. Satellite peaks due to superlattice structure are observed[19] with positions determined by

$$2 \sin \theta / \lambda = 1/\bar{d} \pm n/\Lambda, \qquad (1)$$

where n is the order of the satellite around the main Bragg peak and $\bar{d} = \Lambda/(N_1 + N_2)$, with Λ as the bilayer thickness. In addition, the positions of the peaks in the low angle spectrum are given by[20]

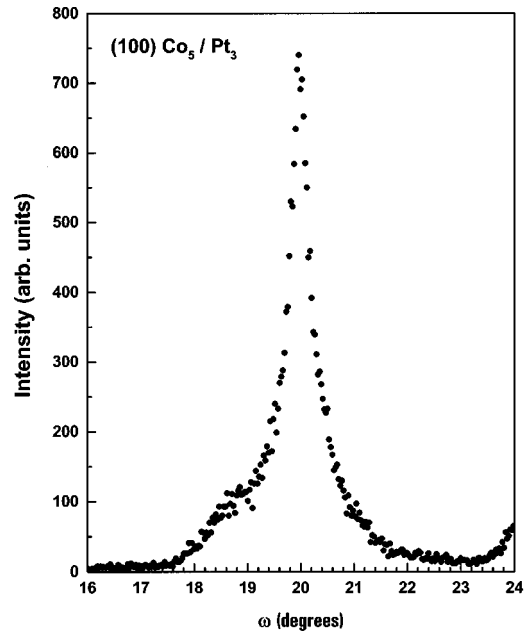$$\sin^2 \theta (n\lambda/2\Lambda)^2 + 2\delta_s, \qquad (2)$$

FIG. 2. Rocking curve performed on the (200) line of a Co_5/Pt_3 superlattice. A full width at half maximum of 0.5° represents very good crystallinity.

where n is the order of the reflection and $1 - \delta_s$ is the real part of the average index of reflection of the superlattice. Λ, determined from our fitting using Eqs. (1) and (2), is within 5% of our designed value. Figure 2 shows a typical rocking curve for the (200) peak whose width reflects the angular distribution of crystallites in the superlattice.[21] The width at half maximum is about 0.5°. This width compares favorably with other metallic superlattices.[22]

We have also performed quantitative analysis on the x-ray-diffraction patterns in order to evaluate interface quality, thickness fluctuations, and the degree of strain. This was done for a series of (111) Co/Pt superlattices with a variety of layer thicknesses. In Fig. 3 we compare the actual x-ray patterns and simulated patterns based on a refined step model incorporating strain and layer thickness variation.[23] It is seen that the simulated patterns accurately reproduce our superlattice spectra. Peak positions, relative intensities, and linewidths are all accounted for by adjusting an interface lattice constant and a thickness distribution width for both the Co and Pt layers. As expected, the interface lattice parameter is approximately given by the weighted average of Co and Pt lattice constants. The broadening of the superlattice peaks was accurately modeled using a Gaussian distribution width of less than 5% of the layer thickness. Finally, the large asymmetry in the intensities of the satellite peaks can be attributed to the 10% lattice mismatch between Co and Pt. Taken together these results verify the excellent layered growth of these Co/Pt superlattices with well-defined (111) and (100) orientation.

IV. MAGNETIC CHARACTERIZATION

It is well known that EHE is very sensitive to the magnetic state of a material. Indeed, it is in direct proportion to the macroscopic magnetization. With this in mind we have measured magnetic hysteresis loops for many of our samples
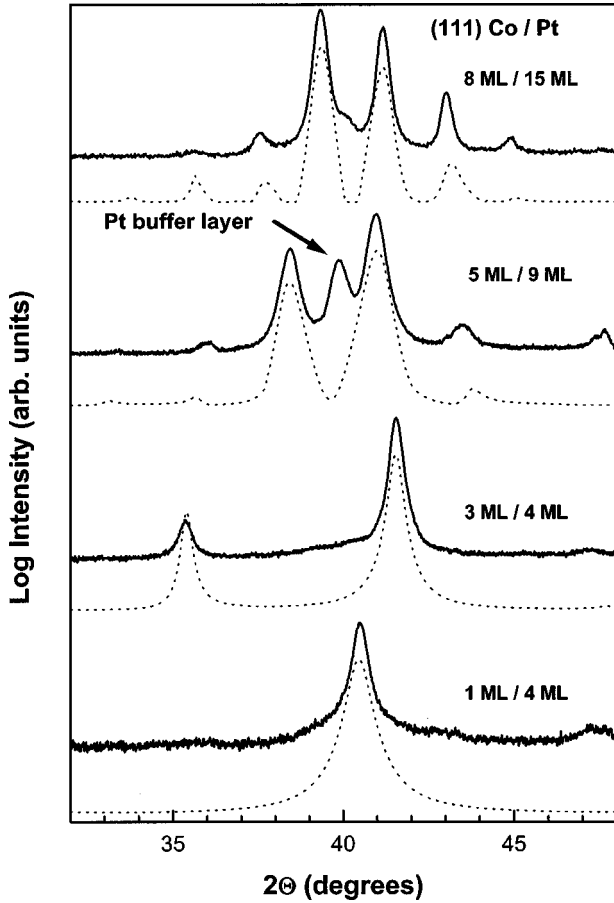
FIG. 3. High angle x-ray-diffraction patterns for a series of (111) Co_{N_1}/Pt_{N_2} superlattices along with fittings generated using a refined step model software package. Note that the intensity is shown in log scale.

FIG. 4. Magnetization loops for perpendicular ($\perp$) and parallel ($\parallel$) configurations of the field (H) with respect to the film plane. The measurements were performed on (111) Co_4/Pt_7 at (a) $T = 5$ K and (b) $T = 300$ K.

with the field either perpendicular or parallel to the plane of the film. We have found that for samples deposited on c-axis oriented Al_2O_3, i.e., (111) Co/Pt superlattices, the magnetization acquires a perpendicular anisotropy as the thickness of the Co layer is decreased. On the other hand, samples deposited on (100) MgO, i.e., (100) Co/Pt superlattices, have only in-plane magnetization. This is consistent with previous reports on Co/Pt superlattices.[22,24] Figure 4 shows the hysteresis loops of a representative (111) Co_4/Pt_7 sample at 5 and 300 K. As is evident this sample has a large perpendicular anisotropy and a nearly 100% remanent magnetization even at 300 K.

The EHE study presented later in this paper will concentrate specifically on two series of (111) orientated samples. For series I, the Pt layer thickness d_{Pt} was held constant at 4 ML's and Co layer thickness d_{Co} varied from 1 to 6 ML's. For series II, d_{Pt} was held constant at 9 ML's and d_{Co} varied from 2 to 7 ML's. We have studied the saturation magnetization M_s and magnetic surface anisotropy of these two series as a function of d_{Co}. The variation of d_{Co} will establish the dependence of both the magnetic properties and EHE on the thickness of the magnetic layer. Further, we expect that not only will d_{Pt} affect the magnetic interlayer coupling and the strain in the magnetic layers and hence the anisotropy characteristics, but also the scaling of EHE, in light of a theory proposed by Zhang[11] and to be discussed later.
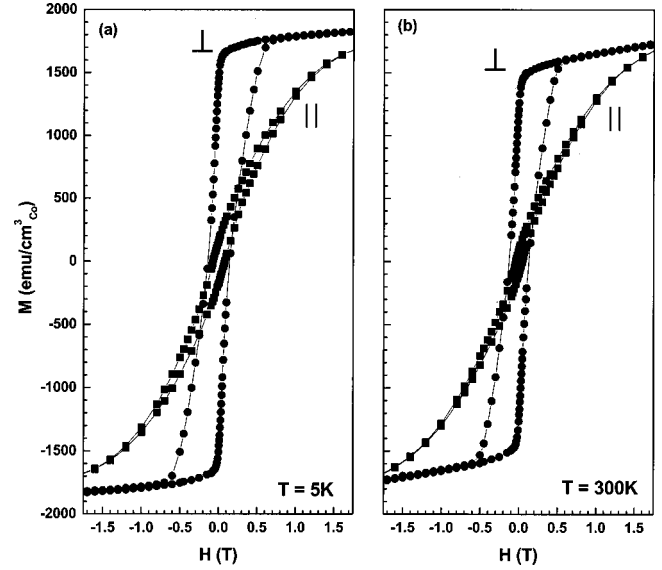
First, we present the results for M_s in Fig. 5 for series II. Shown are perpendicular M vs H curves taken at 5 and 300 K. Parallel curves are shown when available. All samples within this series are saturated more easily with the field in the perpendicular configuration. M_s is obtained by extrapolating $M(H)$ curves from high field to zero field. The error in M_s is within 10%. We have plotted the values of M_s at 5 K, obtained for all samples in both series, in Fig. 6 as a function of inverse Co layer thickness ($1/d_{Co}$). Very interestingly, M_s increases by as much as 55% over the bulk value when d_{Co} is small. The enhancement in M_s is similar to the giant moment phenomenon observed in many magnetic alloy systems, including concentrated CoPt alloys where the effective Co moment μ_{eff} can reach as much as $4.0\mu_B$,[25] as compared to the bulk moment of $1.72\mu_B$. This large effective moment is due to the Co-induced spin polarization on the neighboring Pt atoms.[26]

It is apparent that M_s in Fig. 6 depends linearly on $1/d_{Co}$ for Co layer thickness between 2 and 15 Å, according to

$$M_s = M_0(1 + C/d_{Co}), \quad (3)$$

where M_0 is the bulk magnetization of Co (1446 emu/cm³) at 5 K and $C \sim 1.99$ Å is a constant obtained from the least-square fitting. The $1/d_{Co}$ (surface to volume ratio) dependence of M_s suggests that the induced polarization occurs in the interfacial regions. With this in mind we can construct a simple model of the magnetization characteristics in these superlattices. We assume that all Co atomic layers retain their bulk moment value of μ_0 except for those located at the interfaces. In other words, any enhancement in M_s is confined to the first interfacial Co atomic layer. We assign these interfacial layers an effective moment μ_{eff}, designed to incorporate the large magnetic susceptibility of the Pt neighbors. Based on this simple model we find M_s to follow the linear variation presented above with
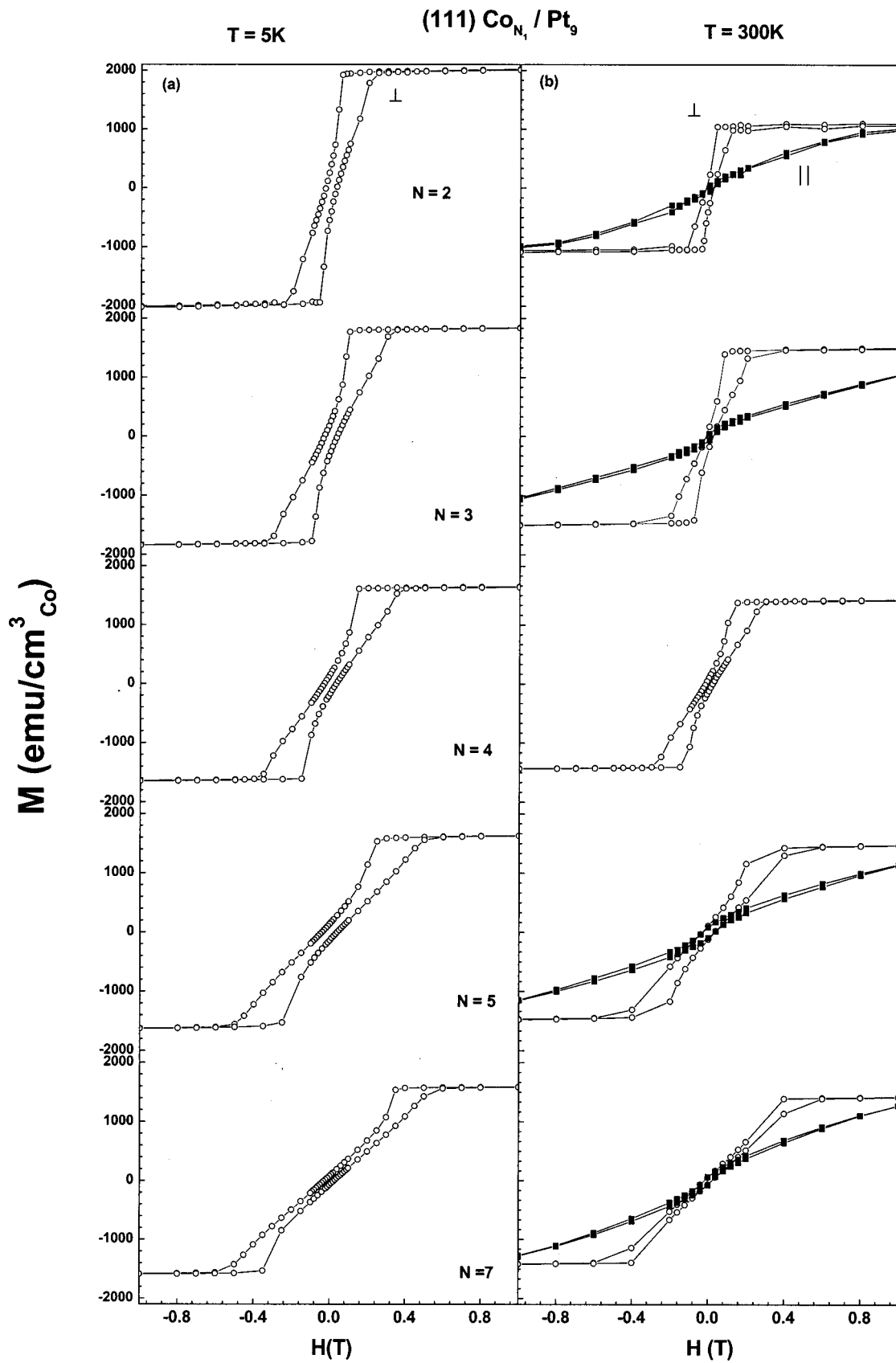
$$C = 2t(\mu_{eff}/\mu_0 - 1), \quad (4)$$

FIG. 5. Compilation of perpendicular magnetization curves for series II, (111) Co_{N_1}/Pt_9 ($N_1 = 2$, 3, 4, 5, 7). Parallel curves are shown when available. The measurements were performed for column (a) at $T = 5$ K and for column (b) at $T = 300$ K. Anisotropy energies were calculated using these plots.
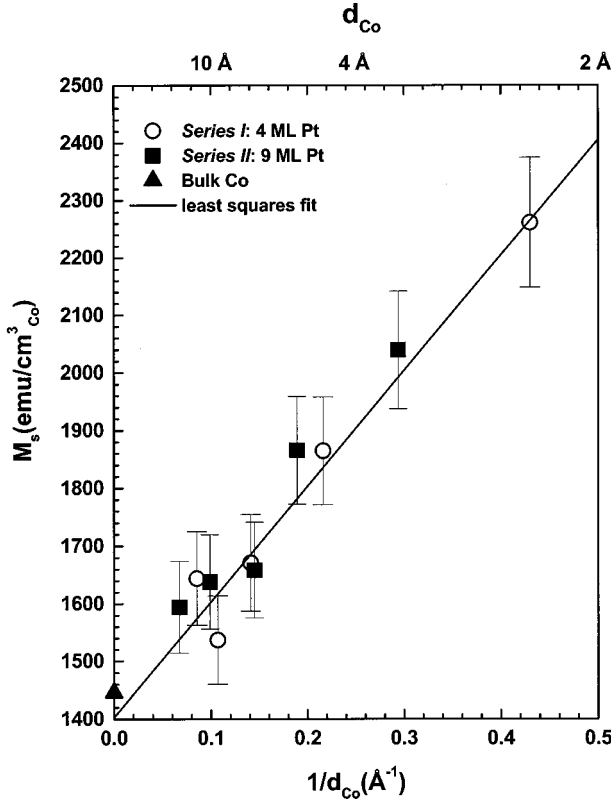
FIG. 6. The saturation magnetization M_s vs $1/d_{Co}$ for series I, (111) Co_{N_1}/Pt_9 ($N_1 = 1, 2, 3, 4, 6$), and series II plotted along with the bulk Co moment of 1446 emu/cm^3. A least-square fit to the data gives $M_s = M_0(1 + C/d_{Co})$ with $C = 1.99$ Å.

FIG. 7. Anisotropy field H_k vs $1/d_{Co}$ for series I and II at $T = 300$ K. A linear dependence both above and below a transition thickness of 5.3 Å suggests an interface anisotropy term may be at play.

where t is the (111) interplanar distance for fcc Co and equals to 2.05 Å. Using the fitted C of 1.99 Å, we find an $\mu_{eff} = 2.56\mu_B$ or an effective magnetization M_{eff} of 2150 emu/cm^3. This compares well with 2250 emu/cm^3 obtained for our thinnest sample ($d_{Co} = 2.3$ Å), which is about 1 ML thick. The enhancement of Co in superlattices is smaller than that in CoPt alloys ($\mu_{eff} = 4.0\mu_B$). We believe this is due to the dimensional effect. For superlattices, polarization occurs only in the two-dimensional interfacial region, whereas alloys offer a quasi-three-dimensional environment for the Co atoms. This allows for a more efficient giant moment formation for Co.

Next, we present our analysis of the magnetic surface anisotropy at 300 K. From Fig. 5 we have obtained the effective anisotropy field H_k, which is the extrapolated intersection of the $H_\parallel$ magnetization curve with the apparent saturation value of the $H_\perp$ curve. In Fig. 7 we plot H_k vs $1/d_{Co}$. A linear dependence of H_k on $1/d_{Co}$ is evident. Note that the linear relationship is valid only over the thickness range 5–15 Å. Below 5 Å, H_k falls off from the straight line. This may be due either to weaker ferromagnetism at 300 K or (as will be discussed later) a coherent to incoherent lattice transition.

Using the magnetization curves in Fig. 5, the magnetic surface anisotropy constant, K_s can be deduced. The net uniaxial magnetic anisotropy, K_u, in these superlattices has contributions from K_s and the volume anisotropy K_ν, which includes the magnetocrystalline anisotropy K_{mc}, the shape anisotropy $(2\pi M_s^2)$, and strain related anisotropies. Phe-

nomenologically, we have the following equation which relates the various anisotropies:[27]

$$K_u d_{Co} = 2K_s + K_\nu d_{Co}. \tag{5}$$

The sign convention is such that positive values of K_u favor out-of-plane magnetization.

Using Eq. (5) we will be able to quantitatively determine the magnitude of the magnetic anisotropy in our superlattices. However, one must pay particular attention to the effect of (tensile) lattice strain σ. Excessive stresses encountered during coherent epitaxial growth may dominate both the in-plane and perpendicular anisotropies. To address this issue we define a critical layer thickness t_c.[26] Below t_c, growth is coherent and lattice misfit is absorbed by elastic strain whereas above t_c growth is incoherent and strain relaxes via misfit dislocations. Following Ref. 26, we can then write down equations for K_s and K_ν in each region. For $d_{Co} < t_c$, it is found that

$$K_s = K_N, \tag{6}$$

$$K_\nu = -2\pi M_s^2 + K_{mc} + K_{me}, \tag{7}$$

where K_N is an interface anisotropy of the Néel type and K_{me} is the magnetoelastic anisotropy. For $d_{Co} > t_c$, it is found that
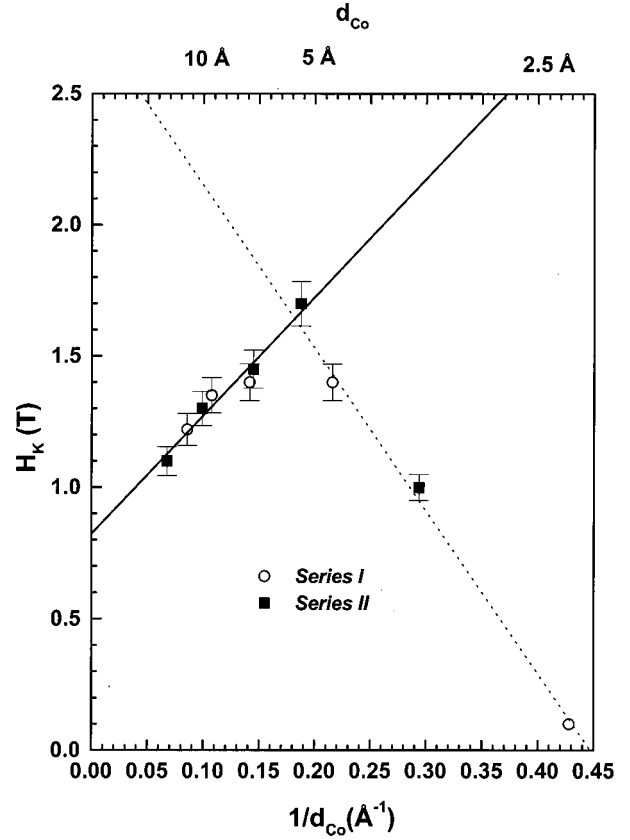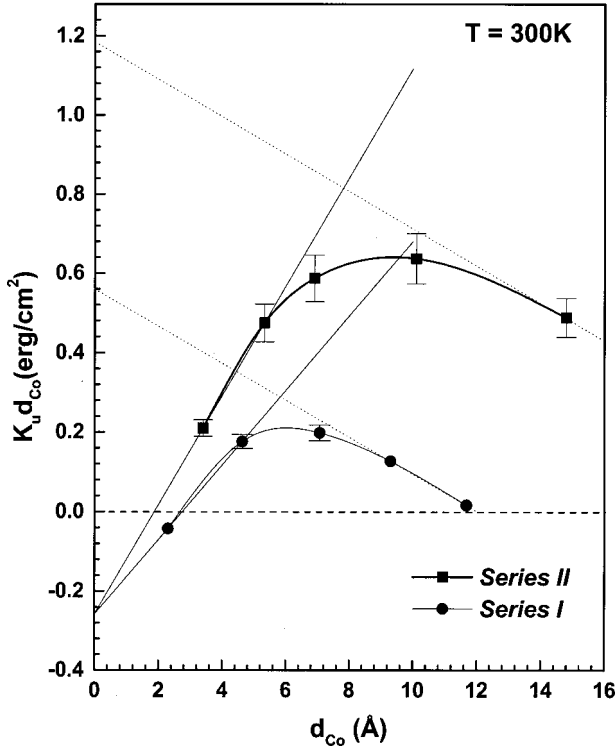
$$K_s = K_N + K_\lambda, \tag{8}$$

FIG. 8. Linear fits to $K_u d_{Co}$ vs d_{Co} both above and below t_c allow the estimation of the anisotropy terms. These are collected in Table I. Series I and II are shown at $T = 300$ K.

$$K_\nu = -2\pi M_s^2 + K_{mc}, \qquad (9)$$

where K_λ is the misfit interface anisotropy. We surmise therefore that for samples differing only in the degree of σ in the Co, controlled perhaps by varying d_{Pt} the anisotropy characteristics can be very different. Indeed, we will discover this to be the case for our two series.

Experimentally, K_u is obtained from the area between the parallel and perpendicular magnetization curves shown in Fig. 5. In Fig. 8 we plot $K_u d_{Co}$ vs d_{Co} for series I and II. Our estimations of the various contributing anisotropies along with values for t_c appear in Table I. The proximity of d_{Co} to t_c in many of our samples requires that our results be considered only approximate. It is difficult to compare with other investigators[22,28] due to the extreme sensitivity of the anisotropy constants upon σ. However, K_ν above t_c and K_N should be independent of σ. Typically, we find a discrepancy of approximately 50% for K_ν and no reported values of K_N. This discrepancy could in principle be attributed to many sources. For instance, a variety of different deposition techniques were used, magnetron sputtering in our case and molecular-beam epitaxy or electron-beam evaporation in the other reports.

Referring the reader to Table 1 and Fig. 8, we make the following observations. First, what is clear is that stress induced anisotropies play a large role in determining PMA. Series II which has a larger d_{Pt} and an associated appreciable σ in the Co has greater values of both K_{me} and K_λ. Further, t_c occurs at a value nearly 2 Å thicker. Most noticeable, K_s is dominated by K_λ above t_c, K_N being both small and negative, and K_{me} is very large, comparable to K_{mc}. These observations confirm that PMA is stress induced in our Co/Pt superlattices.

V. EXTRAORDINARY HALL EFFECT

The Hall effect of a magnetic material depends not only on its electronic structure, but also on the magnetic state. Empirically, the Hall resistivity ρ_{xy} is the sum of an ordinary Hall effect component and an extraordinary Hall effect component,

$$\rho_{xy} = R_0[H + 4\pi M(1-N)] + R_s 4\pi M, \qquad (10)$$

where H is the applied field, M the macroscopic magnetization, N the demagnetization factor, R_0 the ordinary Hall coefficient, and R_s the extraordinary Hall coefficient. Two mechanisms, skew scattering (SS) and quantum side jump (QSJ), are responsible for EHE.[10] Both mechanisms are due to spin-orbit coupling. The SS can be described within a classical Boltzmann approach and is caused by the broken left-right symmetry in scattering. The QSJ is a quantum-mechanical effect and is due to a finite lateral displacement, $\Delta y \sim 0.1$–1 Å, of the electron upon scattering. Theoretical descriptions of the electron scattering in these magnetic systems have borne out a simple relation between R_s and the ordinary resistivity ρ_{xx}, namely,[10]

$$R_s \propto \rho_{xx}^\nu. \qquad (11)$$

Further, it is predicted that SS obligates an exponent ν equal to 1 whereas QSJ requires that $\nu = 2$. SS should then vary linearly with inverse mean free path (MFP) whereas QSJ should depend quadratically on inverse MFP. Hence the scattering will be dominated by SS at low T and QSJ at higher T. These results have been confirmed by many experimental studies performed on diluted and concentrated magnetic alloys.[29]

Superlattices offer a much different magnetic environment for the EHE. The early work has focused primarily on three-dimensional homogeneous alloys. It remains to be seen whether or not the quasi-two-dimensional heterogeneous situation of the superlattice will require a different treatment. Preliminary evidence suggests modification of the early theories is necessary.[11–16] However, a lack of systematics has prevented a clear interpretation of these results. We address

TABLE I. Magnetic anisotropy parameters for series I and II.

Series	t_c (Å)	K below t_c	K above t_c	Stress anisotropy
I (4-ML Pt)	5.86	$K_N = -0.13$ erg/cm^2	$K_S = 0.28$ erg/cm^2	$K_\lambda = 0.41$ erg/cm^2
		$K_V = 9.3 \times 10^6$ erg/cm^3	$K_V = -4.7 \times 10^6$ erg/cm^3	$K_{ME} = 1.4 \times 10^7$ erg/cm^3
II (9-ML Pt)	7.78	$K_N = -0.33$ erg/cm^2	$K_S = 0.59$ erg/cm^2	$K_\lambda = 0.72$ erg/cm^2
		$K_V = 1.4 \times 10^7$ erg/cm^3	$K_V = -4.7 \times 10^6$ erg/cm^3	$K_{ME} = 1.8 \times 10^7$ erg/cm^3

TABLE II. Transport and magnetic properties for series I and II.

Sample ID#	ML co	ν	b (QSJ) $[10^{-4}\,\mu\Omega\,\text{cm}^{-1}\,\text{T}^{-1}]$	a (SS) $[10^{-3}\,\text{T}^{-3}]$	ρ_{xx} (300 K) $[\mu\Omega\,\text{cm}]$	ρ_{xx} (300 K)/ ρ_{xx} (5 K)	R_s (300 K) $[10^{-2}\,\mu\Omega\,\text{cm/T}]$	R_0 (300 K) $[10^{-5}\,\mu\Omega\,\text{cm/T}]$	M_s (5 K) $[\text{emu/cm}^3]$
Series II (9-ML Pt)									
s202b	2	2.67	0.17	−1.12	26.86	2.75	9.59	1.5	2040
s203b	3	2.28	0.25	−1.04	28.93	2.47	18.15	0.15	1866
s204b	4	2.21	0.30	−0.99	30.13	2.60	24.50	0.55	1658
s206b	6	2.13	0.34	−0.76	29.78	2.02	28.02	2.15	1638
s207b	7	2.08	0.35	−0.33	29.76	2.57	30.15	1.45	1594
Series I (4-ML Pt)									
s232a	1	2.31	0.11	−0.31	29.18	5.6	8.37	1.88	2262
s229a	2	2.09	0.23	−0.26	29.15	5.65	18.77	1.57	1865
s226a	3	2.07	0.33	−0.29	32.41	4.86	33.79	1.61	1671
s230a	5	1.99	0.30	0.05	30.79	5.00	29.02	0.86	1537
s231a	6	1.97	0.33	0.19	30.54	4.64	31.10	1.45	1644

this issue by preparing a series with a systematic variation of d_{Co}, a parameter which affects the magnetic dimensionality of the system. Additionally, the Pt thickness, which influences not only the lattice structure of the magnetic layers but also their magnetic properties, is varied to determine its contributions to EHE.

We have measured the Hall resistivity ρ_{xy} and the ordinary resistivity simultaneously as a function of field and temperature. ρ_{xx} was found to change very little with applied field, representing a magnetoresistance (MR) on the order of only 1% at fields of nearly 1 T. Room-temperature resistivities for the two series of samples range from 29 to 31 $\mu\Omega$ cm with resistance ratios (RR), ρ_{xx} (300 K)/ρ_{xx} (4.2 K), ranging from 2.5 for series II to 5 for series I. Table II provides a summary of these results and some other relevant coefficients. These numbers are indicative of good superlattices where disorder induced resistivities are small. However, it should be noted that there does not appear to be any strik-
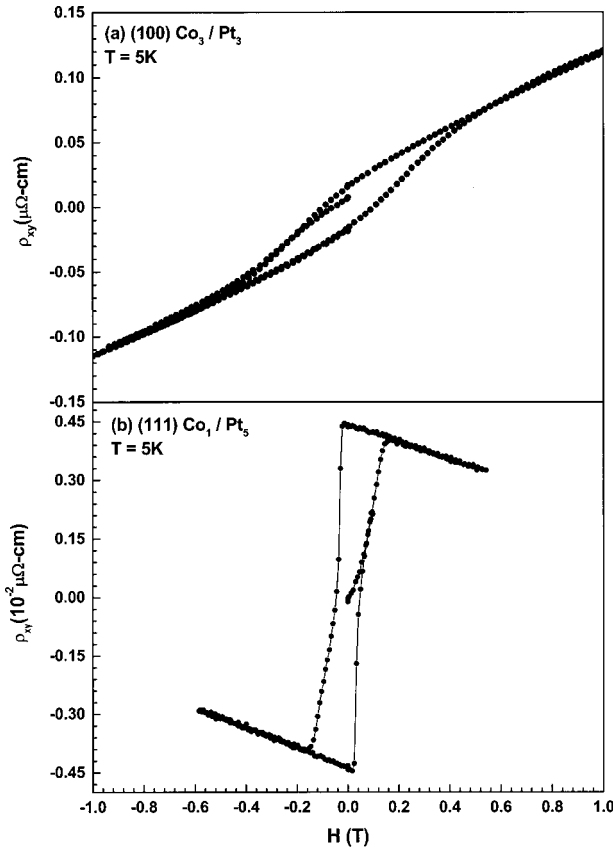

FIG. 9. Typical Hall loops for our Co/Pt superlattices. ρ_{xy} vs H is plotted for (a) (100) Co_3/Pt_3 and (b) (111) Co_2/Pt_5. $T=5$ K for both measurements. Both orientations seem to follow closely their respective $M(H)$ curves.
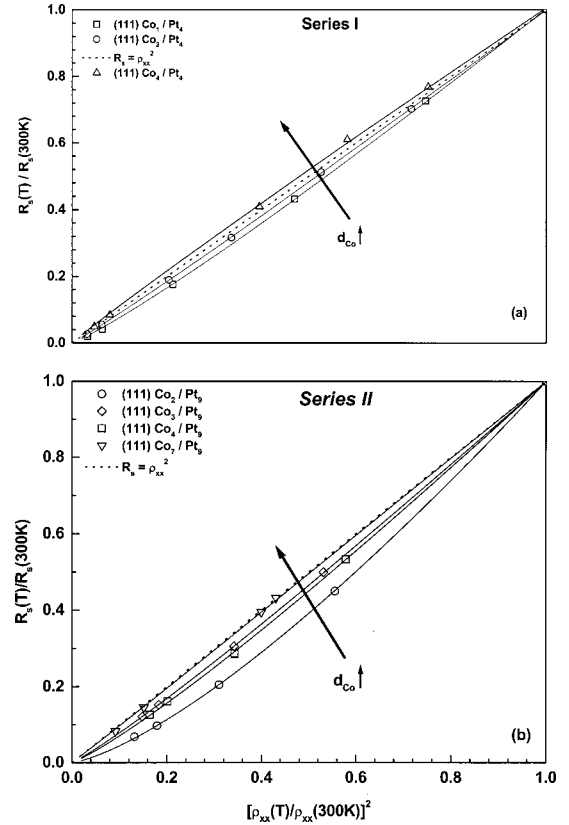

FIG. 10. $R_s(T)/R_s(300\,\text{K})$ vs $[\rho_{xx}(T)/\rho_{xx}(300\,\text{K})]^2$ for a few samples in (a) series I ($N_1=1, 2, 4$) and (b) series II ($N_1=2, 3, 4, 7$). A large discrepancy from the quadratic scaling law is noted for both series. (The long arrow points in the direction of increasing d_{Co}).

$$R_s = A\rho^\nu$$

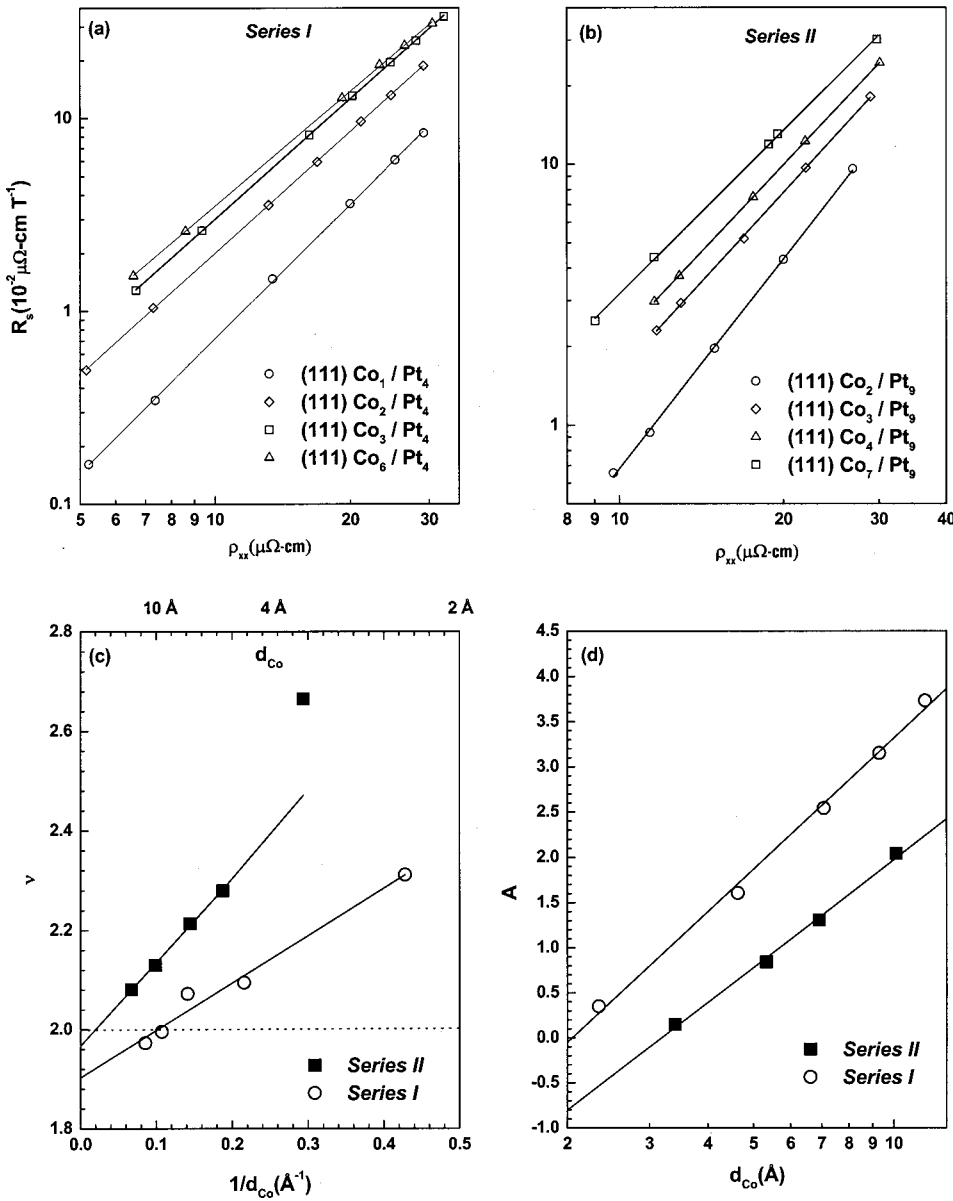

FIG. 11. Investigation of the relation $R_s = A\rho_{xx}^\nu$. A log-log plot of $R_s(T)$ vs $\rho_{xx}(T)$ for (a) series I ($N_1 = 1, 2, 3, 6$) and (b) series II ($N_1 = 2, 3, 4, 7$). T is varied from 4.2 to 300 K. Least-squares fits to the data give ν (slope) and A (log of intercept) for each sample. Their dependencies on d_{Co} are shown in (c) ν vs $1/d_{Co}$ and (d) A vs d_{Co} (log scale).

ing variation of ρ_{xx} with d_{Co} at either 5 or 300 K. Upon closer inspection though, at 5 K for series I, we do indeed observe a nearly linear decrease in ρ_{xx} with increasing d_{Co}, though the effect is small ($\sim 15\%$ change). For series II the smaller RR indicates the relatively larger influence of impurity and disorder scattering on ρ_{xx}, masking any systematic variation with d_{Co}. In either case, it appears that interfacial scattering is not contributing significantly to ρ_{xx} especially at 300 K. This is to be contrasted with results presented later which clearly demonstrate the dramatic effect of the interfacial scattering on the scaling laws. Presumably, the spin-dependent scattering mechanisms are much more strongly dependent on the interfaces in the system. The relative insensitivity of ρ_{xx} on d_{Co} is then consistent with the observed low MR value.

In Fig. 9 we show two representative Hall loops for (100) Co_3/Pt_3 and (111) Co_1/Pt_5. The measurement was done at 5 K. For (100) Co_3/Pt_3 the Hall resistivity shows slightly hys-

teretic behavior below $H = 0.4$ T and then increases linearly with field thereafter, showing no signs of saturation even at the highest field of 1 T. For (111) Co_1/Pt_5 the Hall resistivity remains 100% remnant at zero field with a saturation field of $H = 0.19$ T. Both orientations followed their magnetization loops closely and could be described using the empirical formula

$$\rho_{xy} = R_0 H + R_s 4\pi M, \qquad (12)$$

where we have set the demagnetization factor $N = 1$ for thin-film geometry and assumed R_s to be independent of field so that ρ_{xy} is given simply as a linear combination of an ordinary component proportional to H and an extraordinary component proportional to M. Note that for sample (111) Co_1/Pt_5 the negative slope after saturation due to the normal Hall effect. For most of our samples this effect was small, ranging from -0.5×10^{-12} Ω cm/G at 5 K to near 3×10^{-12} Ω cm/G at room temperature.
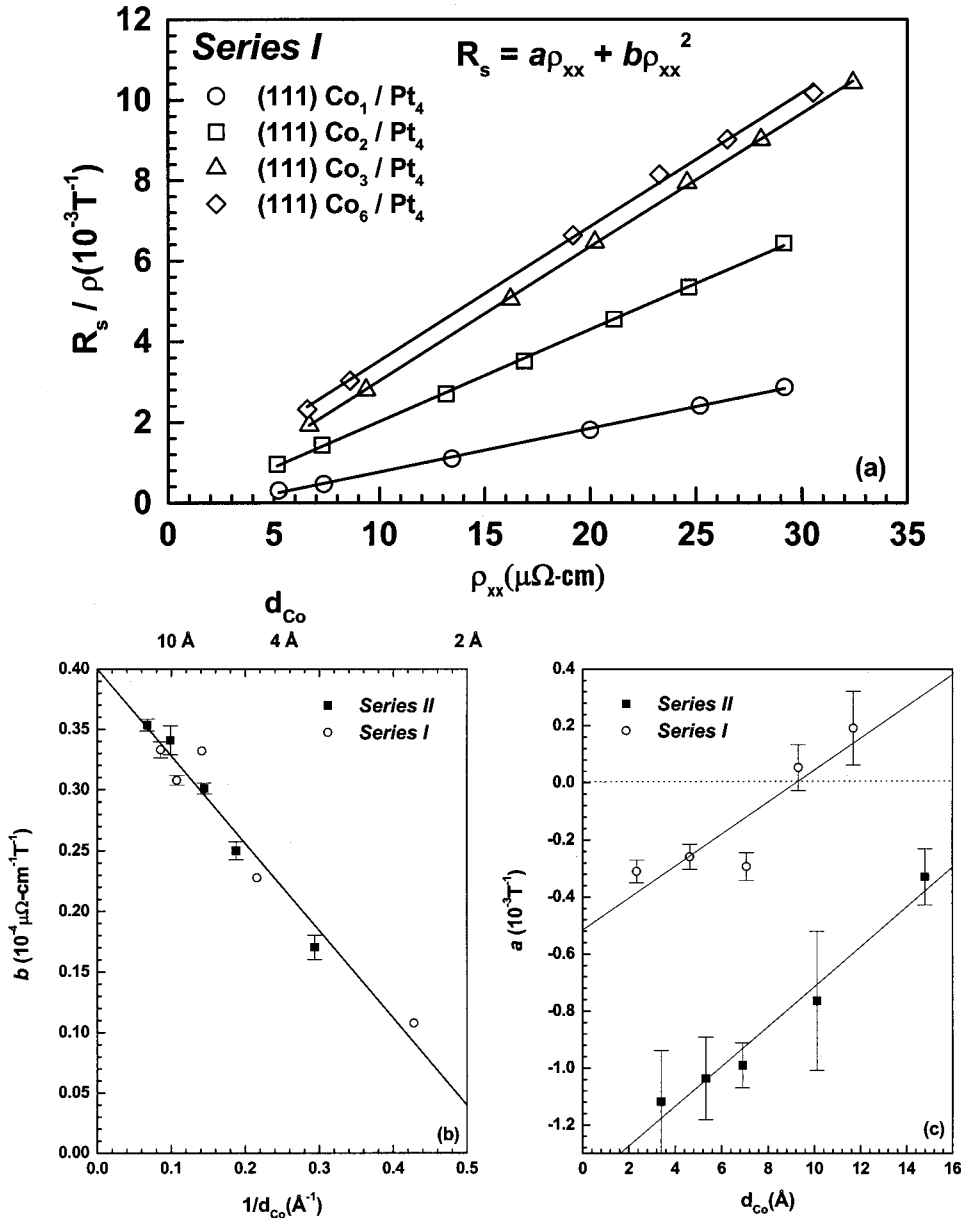
FIG. 12. Investigation of the relation $R_s = a\rho_{xx} + b\rho_{xx}^2$. We show in (a) a plot of $R_s(T)/\rho_{xx}(T)$ vs $\rho_{xx}(T)$ for series I ($N_1 = 1, 2, 3, 6$) for five to six different temperatures (4.2–300 K). Least-square fits to the data give values for the QSJ parameter b (slope) and SS parameter a (intercept) for each sample. Their dependencies on d_{Co} are shown in (b) b vs $1/d_{Co}$ and (c) a vs d_{Co}.

From the Hall resistivity data we were able to extract $R_s(T)$ for series I and II at 5–6 different temperatures and explore its scaling relationship with $\rho_{xx}(T)$ obtained at the same temperatures. To begin, we plot $R_s(T)/R_s$ (300 K) vs $[\rho_{xx}(T)/\rho_{xx}(300 \text{ K})]^2$ for series I and II [Figs. 10(a) and (b)]. Both series reflect similar behavior. For samples with thick d_{Co} (more bulk like), the exponent ν is nearly 2. Here QSJ is the dominant mechanism. However, as d_{Co} is decreased (quasi-two-dimensional limit), there arises a large deviation from the quadratic scaling law, a possible indication of the invalidity of the theory in this regime. Further, there do appear several discrepancies of note in the characteristics of the two series. First, the curves of series I collapse onto the $R_s = \rho_{xx}^2$ line much more quickly. And second, series II supports curves with much larger deviations from the quadratic scaling. As we will see later, this may be due to a larger relative difference between d_{Co} and d_{Pt}. However, for both series the curves are reminiscent of Zhang's theoretical work.[11]

To ascertain whether a different scaling relation is at play

we have further analyzed our data according to Figs. 11(a) and (b). Here we present log-log plots of $R_s(T)$ vs $\rho_{xx}(T)$ for series I and II, respectively. The slope is then given simply by ν and the intercept by the log of a proportionality constant A in Eq. (11). Our data fit very well to Eq. (11) for both series over a large temperature range (4.2–300 K). As d_{Co} is varied there is a systematic change of both ν and A. Figures 11(c) and (d) highlight this variation. Over the entire thickness range ν depends linearly on $1/d_{Co}$. This is an indication that interfacial scattering may be dominating the Hall effect, and indeed for this thickness regime we would expect such to be the case. Further, in series I the intersection with the horizontal line $\nu = 2$ (QSJ) occurs at $d_{Co} \sim 9.5$ Å, with two samples actually having an exponent slightly less than 2. This is in contrast to series II which extrapolates to an intersection with $\nu = 2$ at $d_{Co} \sim 20$ Å. Interestingly, both intersection points occur when $d_{Co} \sim d_{Pt}$. Equally fascinating, A depends on $\log(d_{Co})$ in a linear fashion for both series. As a consequence, the scaling relationship in our Co/Pt superlattices is parametrized by the sole variable d_{Co}.

The smooth variation of the fitting parameters across the thickness range measured may seem inconsistent in light of the behavior observed in the anisotropy characteristics. In particular, we see no discrepancies owing to the coherent to incoherent transition. One might expect such a structural transition to strongly influence any interface scattering. However, the spin-dependent scattering is affected by the local magnetic environment, whereas the magnetic anisotropy depends on long-range inhomogeneity (e.g., dislocations). Assuming the dislocations are well separated from each other, the local magnetic environment does not change significantly as a result of this transition and so we observe smooth variation in the fitting parameters.

To elucidate the physics behind these correlations we will need to first summarize the findings of Zhang (Ref. 11). Up until this time there had been no previous attempts to model the spatial and spin inhomogeneities associated with super-lattices within the context of EHE. Zhang, by using the Kubo formalism, is able to show that the commonly used scaling relation is not valid for superlattices. In particular, he focuses on QSJ, which should be the main source for EHE because of the higher resistivities associated with multilayered structures. The derived Hall conductivity σ_{xy} is found to depend on the strength and range of the scattering potentials in the system (in direct contrast to homogeneous systems). Zhang's explanation is that the relevant parameters, such as MFP, have become spatially varying. The electron sees an inhomogeneous scattering environment. If, however, MFP is much less than the layer thickness, i.e., the local limit, the situation reduces to the homogeneous case because the electrons are never made aware of the inhomogeneities in the system and the scaling law is re-established. Whereas when the MFP is much larger than the layer thickness, i.e., long MFP limit, the electron samples many layers before scattering. In this case Zhang finds that $\sigma_{xy}(=\rho_{xy}/\rho_{xx}^2)$ depends on the ratio of the relaxation times in the magnetic layers and nonmagnetic layers. This can be compared to the earlier results[10] where σ_{xy} is found to be proportional to Δy which is independent of the scattering potential or the relaxation time. Numerical analysis reveals that the exponent in the scaling law can be smaller, greater or equal to 2, depending on the relative variations in the MFP for the magnetic and nonmagnetic layers.

In much of Zhang's analysis interface scattering is neglected for simplicity. However, our results suggest it is the dominant scattering mechanism for samples with d_{Co} between 2 and 15 Å and d_{Pt} from 9 to 20 Å. This prohibits any quantitative comparison with Zhang's model. However, qualitatively our results are very similar. If we assume that the interfaces dominate the scattering, which is reasonable, then the MFP in the superlattice will be determined primarily by the Co/Pt interfaces. We can then argue that the MFPs will scale as the layer thicknesses so long as the linear variation of $1/d_{Co}$ with ν holds. The MFP will then systematically change with d_{Co} for each series. In our samples with very small d_{Co} the MFP will be very different in the cobalt and the platinum layers. And we expect deviation from the scaling law, as explained by Zhang. As we increase d_{Co} we approach the quadratic scaling law linearly with $1/d_{Co}$. And as we noted above when $d_{Co} \sim d_{Pt}$ i.e., when the MFP's are almost equal, then $\nu = 2$. Once d_{Co} becomes greater than d_{Pt}
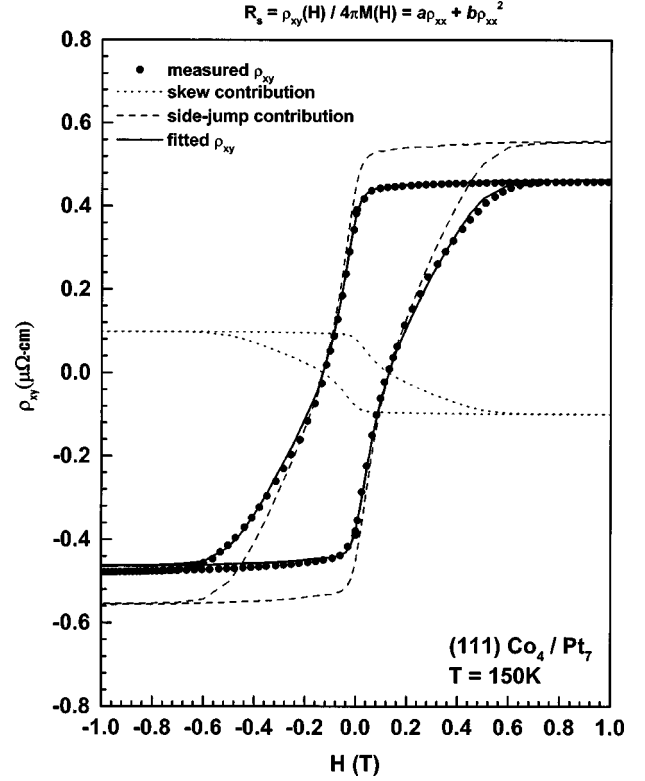

FIG. 13. The result of the fitting $\rho_{xy}(H) = (a\rho_{xx} + b\rho_{xx}^2) M(H)$ using the measured $\rho_{xy}(H)$ and $M(H)$ curves for Co$_4$/Pt$_9$ at $T = 150$ K. The individual contributions from SS, $[a\rho_{xx}M(H)]$, and QSJ, $[b\rho_{xx}^2 M(H)]$, are superimposed upon the fitting.

the exponent deviates from 2 once again but this time it becomes smaller. We suspect that as d_{Co} or d_{Pt} increase further other scattering mechanisms will become important and deviation from the $1/d_{Co}$ dependence of ν will arise. A correct theoretical treatment of the problem will need to include the effect of interface scattering, which seems to be the crucial mechanism controlling MFP of the electrons.

Thus far, we have been working under the assumption that QSJ was dominating the scattering in our superlattices. Though this may well be the case, we wish to further analyze our results by adding a contribution from SS and resorting to the old scaling relations. Within the context of the original theories on EHE developed by Luttinger and Berger[10] we would expect the two terms to add linearly to give the following relation:

$$R_s = a\rho_{xx} + b\rho_{xx}^2, \qquad (13)$$

where a is the SS constant and b is the QSJ constant. Assuming the parameters a, b are independent of temperature we expect a linear variation of $R_s(T)/\rho_{xx}(T)$ with $\rho_{xx}(T)$. The results of such an analysis are presented in Fig. 12(a), where we show $R_s(T)/\rho_{xx}(T)$ vs $\rho_{xx}(T)$ curves for series I. Our data fit very well to Eq. (13) and show a systematic variation as d_{Co} is increased. From least-square fits we have determined a, b independently and plotted their dependence on d_{Co} [Figs. 12(b) and (c)]. The QSJ parameter b varies linearly with $1/d_{Co}$ and is *independent* of series. We then conclude that QSJ is dominated by interface scattering and is insensitive to the nonmagnetic layer thickness. The SS pa-

rameter a varies approximately linearly with d_{Co} and does depend on series. For series II, SS contribution is always negative whereas in series I, a reaches zero at roughly 9 Å and then becomes positive for larger d_{Co}.

To get a better idea of the relative contributions of the two mechanism we have plotted in Fig. 13 a fit to ρ_{xy} using the experimentally determined $M(H)$ and $\rho_{xy}(H)$ curves and a knowledge of the field independent coefficients a and b (note that we have ignored the normal Hall component due to its very small effect). The relative contributions from the SS component and the QSJ component are superimposed upon the fitting. The $M(H)$ curve is well reproduced by this method both above and below the saturation field. Apparently then, once a knowledge of a and b is acquired there is no need to measure M and ρ_{xy} independently. Note that a small negative SS contribution combines with a large QSJ component to generate the total ρ_{xy}. The measurement was done at 150 K for sample (111) Co_4/Pt_9.

VI. CONCLUSIONS

Well-orientated and highly crystalline (111) and (100) Co/Pt superlattices have been fabricated. Those samples with (100) orientation were found to have in-plane magnetization to which the EHE closely corresponded. (111) orientated superlattices were seen to exhibit a large PMA in a certain thickness range which was determined by the degree of tensile strain present in the Co layers. A systematic investigation of two series of (111) orientated samples with similar d_{Co} variations but rather different values of d_{Pt} revealed an enhancement of the Co moment in the interfacial region by roughly 55% over the bulk value. In addition, an interface anisotropy of strain related origins was observed. Series II, with a larger tensile strain, had a larger and more robust PMA. The EHE characteristics of the two series were also different. If we assumed that only QSJ contributed to EHE then our analysis revealed a deviation from the normal scaling relations reminiscent of Zhang's theory. However, interfacial scattering was recognized as the dominant scattering mechanism so any qualitative comparison with Zhang, who ignored this term for simplicity, would be erroneous. Further, it was noticed that both series intersected with the quadratic scaling law when $d_{Co} \sim d_{Pt}$, and we argued that this was because of an equilibration of MFP in the Co and Pt layers. If SS was also assumed to be at play in our Co/Pt superlattices then the old scaling laws became an accurate representation of our data. Interface scattering was also prevalent in the QSJ term. We suspect that the inhomogeneous environment of the superlattice does require an additional treatment and that the agreement with the scaling relations derived for homogeneous systems is fortuitous. What is clear though, is that any theory which attempts to model EHE in superlattices will have to take into account the large role played by the interfaces.

---

*Present address: Physics Department (MRSEC), University of Maryland, College Park, MD 20742.

†Present address: Seagate Recording Media, 47010 Kato Road, Fremont, CA 94538.

[1] See, e.g., Phys. Today **48** (4), 58 (1995).

[2] For a review, See Appl. Phys. A: Solids Surf. **A49**, (1989).

[3] C. Chappert, K. LeDang, P. Beauvillain, H. Hurdequint, and D. Renard, Phys. Rev. B **34**, 3192 (1986); C. H. Lee, Hui He, F. Lamelas, W. Vavara, C. Uher, and Roy Clarke, Phys. Rev. Lett. **62**, 653 (1989).

[4] D. Pescia, G. Zampieri, M. Stampanoni, G. L. Bona, R. F. Willis, and F. Meier, Phys. Rev. Lett. **58**, 933 (1987); F. J. Lamelas, C. H. Lee, Hui He, W. Vavra, and Roy Clarke, Phys. Rev. B **40**, 5837 (1989).

[5] N. C. Koon, B. T. Jonker, F. A. Volkening, J. J. Krebs, and G. A. Prinz, Phys. Rev. Lett. **59**, 2463 (1987); J. R. Dutcher, J. F. Cochran, B. Heinrich, and A. S. Arrott, J. Appl. Phys. **64**, 6095 (1988).

[6] W. B. Zeper, J. A. M. Greidanus, P. F. Carcia, and C. R. Fincher, J. Appl. Phys. **65**, 4971 (1989).

[7] F. J. A. edn Broeder, D. Kuiper, H. C. Donkersloot, and W. Hoving, Applied Physics A, Solids **49**, 507 (1989).

[8] R. Schad, C. D. Potter, P. Beliën, G. Verbanck, V. V. Moshchalkov, and Y. Bruynseraede, Appl. Phys. Lett. **64**, 3500 (1994).

[9] R. J. Gambino and T. R. McGuire, IBM Tech. Discl. Bull. **18**, 4214 (1976).

[10] L. Berger and G. Bergmann, in *The Hall Effect and Its Applications*, edited by C. L. Chien and C. R. Westgate (Plenum, New York, 1979).

[11] Shufeng Zhang, Phys. Rev. B **51**, 3632 (1995).

[12] S. N. Song, C. Sellers, and J. B. Ketterson, Appl. Phys. Lett. **59**, 479 (1991).

[13] W. Vavra, C. H. Lee, F. J. Lamelas, H. He, R. Clarke, and C. Uher, Phys. Rev. B **42**, 4889 (1990).

[14] H. Sato, T. Kumano, Y. Aoki, T. Kaneko, and R. Yamomoto, J. Phys. Soc. Jpn. **62**, 416 (1993).

[15] F. Tsui, B. Chen, D. Barlett, R. Clarke, and C. Uher, Phys. Rev. Lett. **72**, 740 (1994).

[16] P. Xiong, G. Xiao, J. Q. Wang, J. Q. Xiao, J. S. Jiang, and C. L. Chien, Phys. Rev. Lett. **69**, 3220 (1993).

[17] S. Hashimoto, A. Maesaka, K. Fujimoto, and K. Bessho, J. Magn. Magn. Mater. **121**, 471 (1993).

[18] P. F. Carcia, Z. G. Li, and W. B. Zeper, J. Magn. Magn. Mater. **121**, 452 (1993).

[19] M. R. Khan, C. S. L. Chun, G. P. Felcher, M. Grimsditch, A. Kueny, C. M. Falco, and I. K. Schuller, Phys. Rev. **27**, 7186 (1983).

[20] P. F. Miceli, D. A. Neumann, and H. Zabel, Appl. Phys. Lett. **48**, 24 (1986).

[21] I. K. Schuller, Solid State Commun. **92**, 141 (1994).

[22] R. F. C. Farrow, C. H. Lee, R. F. Marks, G. R. Harp, and M. F. Toney, in *Magnetism and Structure in Systems of Reduced Dimension*, edited by R. F. C. Farrow, B. Dieny, M. Donath, A. Fert, and B. D. Hermsmeier (Plenum, New York, 1993).

[23] See, e.g., E. E. Fullerton, I. K. Schuller, H. Vanderstraeten, and Y. Bruynseraede, Phys. Rev. B **45**, 9292 (1992).

[24] D. Weller, R. F. C. Farrow, R. F. Marks, G. R. Harp, H. Notarys, and G. Gorman, in *Magnetic Ultrathin Films—Multilayers and*

Surfaces, Interfaces and Characterization, edited by B. T. Jonker, S. A. Chambers, R. F. C. Farrow, C. Chappert, R. Clarke, W. J. M. de Jonge, T. Egami, P. Grünberg, K. M. Krishnan, E. E. Marinero, C. Rau, and S. Tsunashima, MRS Symposia Proceedings No. 313 (Materials Research Society, Pittsburgh, 1993), p. 791; R. H. Victora and J. M. MacLaren, J. Appl. Phys. **73**, 6415 (1993).

[25] J. Crangle and W. R. Scott, J. Appl. Phys. **38**, 921 (1965); G. A. Swallow, G. Williams, A. D. C. Grassie, and J. W. Loram, J. Phys. F: Met. Phys. **1**, 511 (1971).

[26] J. A. Mydosh and G. J. Nieuwenhuys, in *Ferromagnetic Materi-*

als I, edited by E. P. Wohlfarth (North-Holland, New York, 1980).

[27] M. T. Johnson, R. Jungblut, P. J. Kelly, and F. J. A. den Broeder, J. Magn. Magn. Mater. **148**, 118 (1995).

[28] W. B. Zeper, F. J. A. M. Greidanus, P. F. Carcia, and C. R. Fincher, J. Appl. Phys. **65**, 4971 (1989).

[29] W. Jellinghaus and M. P. DeAndres, Ann. Phys. (Leipzig) **7**, 189 (1961); C. Kooi, Phys. Rev. **95**, 843 (1954); J. P. Jan, Helv. Phys. Acta **25**, 677 (1952); W. Köster and O. Römer, Z. Metallkd. **55**, 805 (1964).